# Statistics and Dynamics of Aircraft Encounters of Turbulence over Greenland

TODD P. LANE

*The University of Melbourne, Melbourne, Australia*

JAMES D. DOYLE

*Naval Research Laboratory, Monterey, California*

ROBERT D. SHARMAN

*National Center for Atmospheric Research,* Boulder, Colorado*

MELVYN A. SHAPIRO

*University of Bergen, Bergen, Norway, and Cooperative Institute for Research in Environmental Sciences, University of Colorado and the National Oceanographic and Atmospheric Administration, Boulder, Colorado*

CAMPBELL D. WATSON

*The University of Melbourne, Melbourne, Australia*

(Manuscript received 20 November 2008, in final form 5 February 2009)

ABSTRACT

Historical records of aviation turbulence encounters above Greenland are examined for the period from 2000 to 2006. These data identify an important flow regime that contributes to the occurrence of aircraft turbulence encounters, associated with the passage of surface cyclones that direct easterly or southeasterly flow over Greenland's imposing terrain. The result of this incident flow is the generation of mountain waves that may become unstable through interactions with the background directional wind shear. It is shown that this regime accounted for approximately 40% of the significant turbulent events identified in the 7-yr database. In addition, two specific cases from the database are examined in more detail using a high-resolution mesoscale model. The model simulations highlight the important role of three-dimensional gravity wave–critical level interactions and demonstrate the utility of high-resolution forecasts in the prediction of such events.

## 1. Introduction

Mountains and mountain ranges have important influences on the incident atmospheric flow because of the substantial lateral and vertical flow displacements that they induce. Such flow displacements lead to the enhancement or initiation of precipitation (e.g., Roe 2005), the generation of wakes that can control the climatological meteorological conditions (e.g., Smith and Grubišić 1993), and substantial large-amplitude mountain waves and turbulent energy dissipation. Mountain waves and their associated vertical flux of horizontal momentum are significant components in the momentum budget of the middle atmosphere (Fritts and Alexander 2003; Kim et al. 2003) through their modulation of the background flow in regions of momentum flux divergence. One process that causes a divergence of the momentum flux is wave breaking (e.g., Lilly and Kennedy 1973); wave instability and breaking initiates turbulence, which also contributes to the vertical redistribution of atmospheric constituents, such as ozone, water vapor, and aerosols (e.g., Dörnbrack 1998), and poses a hazard to aviation (e.g., Lilly 1978).

* The National Center for Atmospheric Research is sponsored by the National Science Foundation.

*Corresponding author address:* Todd Lane, School of Earth Sciences, The University of Melbourne, Melbourne, VIC 3010, Australia.
E-mail: tplane@unimelb.edu.au

DOI: 10.1175/2009MWR2878.1

# Report Documentation Page

*Form Approved*
*OMB No. 0704-0188*



| 1. REPORT DATE | 2. REPORT TYPE | 3. DATES COVERED |
|---|---|---|
| **AUG 2009** | | **00-00-2009 to 00-00-2009** |

| 4. TITLE AND SUBTITLE | 5a. CONTRACT NUMBER |
|---|---|
| **Statistics and Dynamics of Aircraft Encounters of Turbulence over Greenland** | 5b. GRANT NUMBER |
| | 5c. PROGRAM ELEMENT NUMBER |
| 6. AUTHOR(S) | 5d. PROJECT NUMBER |
| | 5e. TASK NUMBER |
| | 5f. WORK UNIT NUMBER |
| 7. PERFORMING ORGANIZATION NAME(S) AND ADDRESS(ES) **The University of Melbourne ,Melbourne, Australia, , ,** | 8. PERFORMING ORGANIZATION REPORT NUMBER |
| 9. SPONSORING/MONITORING AGENCY NAME(S) AND ADDRESS(ES) | 10. SPONSOR/MONITOR'S ACRONYM(S) |
| | 11. SPONSOR/MONITOR'S REPORT NUMBER(S) |

12. DISTRIBUTION/AVAILABILITY STATEMENT
**Approved for public release; distribution unlimited**

13. SUPPLEMENTARY NOTES

14. ABSTRACT

15. SUBJECT TERMS

| 16. SECURITY CLASSIFICATION OF: | | | 17. LIMITATION OF ABSTRACT | 18. NUMBER OF PAGES | 19a. NAME OF RESPONSIBLE PERSON |
|---|---|---|---|---|---|
| a. REPORT **unclassified** | b. ABSTRACT **unclassified** | c. THIS PAGE **unclassified** | **Public Release** | **17** | |

In a survey of reported encounters between commercial aircraft and turbulence over the contiguous United States, Wolff and Sharman (2008) highlight mechanisms contributing to turbulence generation, as well as identifying preferred locations of turbulence occurrence. In particular, regions of complex terrain, such as the Rocky Mountains, composed the major contribution to the total number of turbulence reports, with the source being attributed to mountain-wave-breaking processes. Other regions around the world that feature frequent air traffic passing above complex terrain also regularly pose a hazard to aviation such as the Alps (e.g., Jiang and Doyle 2004) and Greenland (e.g., Doyle et al. 2005; Ólafsson and Ágústsson 2009). Greenland underlies the preferred flight routes between North America and Europe, and turbulence above Greenland is the focus of this study.

Turbulence derived from interactions with terrain and mountain waves can be due to a variety of processes, including eddy shedding (Clark et al. 1997), rotors (Doyle and Durran 2002), wake effects (Lane et al. 2006), and nonlinear processes associated with large-amplitude and breaking waves (Lilly 1978). In the upper troposphere/lower stratosphere, where surface effects and cloud/precipitation hazards are reduced, wave breaking is probably the most important individual mechanism that affects aviation safety near mountains.

The causes of upper-level wave breakdown are complex, being due to large-amplitude forcing, non-Boussinesq effects, critical levels in the background flow (Booker and Bretherton 1967; Wurtele et al. 1996), wave–wave interactions (Franke and Robinson 1999), and/or nonlinear wave resonance (Peltier and Clark 1983; Bacmeister and Schoeberl 1989; Thorpe 1975, 1987). These processes become particularly elusive when considering the broader spectrum of waves generated by complex topography (e.g., Jiang and Doyle 2004; Sharman and Wurtele 2004) and evolving flow conditions (e.g., Ralph et al. 1992, 1997; Clark et al. 2000). In many cases, processes described by steady-state two-dimensional critical level theory can be invoked to explain the underlying dynamics. In two dimensions, a critical level for stationary mountain waves occurs when the background wind speed equals zero in association with flow reversals or localized minima in wind speed. For example, the 11 January 1972 Boulder windstorm case (Lilly 1978; Doyle et al. 2000) featured a minimum in background zonal wind in the stratosphere, contributing to the formation of wave breaking at upper levels. Simulations of this case by Clark and Peltier (1984) also showed that resonance that resulted in instability and wave breaking occurred well below the background critical level in part due to wave reflection by that critical level. This suggests that wave instability and breaking may be caused *indirectly* by the presence of a critical level, which acts to confine the wave energy below its nominal height and maximizes nonlinear interactions. Furthermore, the negative shear (in the cross-mountain direction) associated with a critical level farther aloft can lead to wave amplification, which may also enhance nonlinearity.

Grubišić and Smolarkiewicz (1997) showed that, in three-dimensional flow, the critical level (for stationary waves) is the height at which the wind is zero when projected onto the same direction as the wave vector. Thus, the concept of a critical level becomes less well defined in common wind conditions that contain both directional and speed shears and regions of complex topography because the appropriate direction of the wave vector is difficult to define and so is the altitude of reversal of the wind in that vector direction (e.g., Shutts 1995; Doyle and Jiang 2006). It is reasonable to assume that the low-level wind defines the predominant direction of the wave vector, and a rotation in the wind of at least 90° will be sufficient to induce a critical level for at least part of the wave spectrum. Thus, for realistic scenarios, using simple theories to forecast turbulence over terrain becomes challenging—suggesting the importance of numerical prediction in future turbulence prediction systems.

There are presently a number of approaches for mountain-wave turbulence prediction and avoidance: (i) ad hoc real-time avoidance facilitated through the use of pilot reports of turbulence encounters; (ii) examination of satellite images for evidence of mountain-wave signatures to diagnose locations of potential mountain-wave turbulence (Uhlenbrock et al. 2007); (iii) the use of sophisticated algorithms utilizing gridded forecast model output (e.g., Bacmeister et al. 1994; Sharman et al. 2006); and (iv) predictions of turbulence directly from high-resolution regional forecast models that explicitly resolve the wave dynamics (e.g., Doyle et al. 2005)—such forecasts could be derived directly from parameterized turbulent kinetic energy or diagnosed using spectral or structure function analysis (Frehlich and Sharman 2004) of the model fields. As computer capacity increases, the latter approach is likely to be the most successful for predictions of terrain-induced turbulence, because the terrain features are known and the prediction does not rely on the skillful representation of aspects of a source that has lesser predictive skill, such as deep moist convection.

Of course, in addition to developing automated approaches to forecasting, there is value in improving knowledge of flow regimes and meteorological conditions that are more conducive to turbulence production.

Turbulence in the vicinity of Greenland is chosen as the focus of this study because of its importance to the trans–North Atlantic flight route and the limited studies to date of turbulence in this region. The objectives of this paper are to (i) explore the variability of turbulence encounters over Greenland and identify important flow regimes contributing to that variability; and (ii) employ a high-resolution mesoscale model to explore the governing dynamics in selected significant case studies. The remainder of this paper is organized as follows: section 2 describes the database of turbulence reports in the vicinity of Greenland, the seasonal distribution, and an important flow regime elucidated by this analysis; two cases are examined and simulated in more detail in section 3; the importance of these results for aviation safety and operations are discussed in section 4; and finally, conclusions are presented in section 5.

## 2. Turbulence statistics (2000–06)

Commercial aircraft routinely report occurrences of turbulence during flight. These reports, referred to as Pilot Reports (PIREPS) over the continental United States and Aircraft Reports (AIREPS) over the oceans, provide an indication of turbulence location and intensity used by air traffic control in real time to monitor turbulence in the airspace. The aircraft pilots assign a subjective measure of the turbulence intensity (TB) that is experienced, ranging from null or smooth to extreme turbulence. These records can be coded on a 0–8 scale as either 0 (null), 1 (smooth to light), 2 (light), 3 (light to moderate), 4 (moderate), 5 (moderate to severe), 6 (severe), 7 (severe to extreme), or 8 (extreme). These reports are issued at any time or location, but are required at least every 10° of longitude (for east–west-oriented oceanic flight routes). With these factors in mind, AIREPS are not without substantial uncertainties. AIREPS are subjective; with the measure of intensity determined by the pilots' own personal experience. AIREPS suffer uncertainty in the spatial location, with recorded locations possibly representing turbulence that was experienced tens or even hundreds of kilometers prior to or after the actual location (Schwartz 1996; Wolff and Sharman 2008). Furthermore, AIREPS usually contain single isolated reports that do not provide information about the longevity of the turbulence encounter. Nevertheless, despite these uncertainties, these turbulence records provide a useful indication of the spatial and temporal variability of turbulence within a given region.

A database of AIREPS was assembled to explore the occurrence and variability of turbulence in the vicinity of Greenland. This database covers the period of January 2000 to December 2006 and is restricted to the geographic area within latitudes of 59°–80°N and longitudes of 65°–25°W; these coordinates surround Greenland (see Fig. 1). Within this database, there are more than 38 000 turbulence reports (including null turbulence), and 1515 reports of moderate or greater (MOG,[1] TB $\geq$ 4) turbulence intensities. These MOG reports occurred on 655 individual days during the 7-yr period, and therefore on average every fourth day has at least one MOG turbulence report. Severe reports are far less frequent, with only 49 severe or greater (TB $\geq$ 6) reports (only 3% of MOG reports) during the 7-yr period. The most MOG reports in any single day (i.e., 36) were reported on 11 January 2003, and on 19 February 2000 the second-most MOG reports (i.e., 33) were reported; these two events are described in detail in section 3.

Our underlying assumption is that the majority of the (MOG) turbulence encounters are the result of interactions between the background flow and the imposing Greenland terrain. Such an assumption is justified, in part, by the results of Wolff and Sharman (2008) who highlight the significant localized enhancement of turbulence reports over the mountainous regions of the contiguous United States. Most of these turbulence reports are probably associated with mountain-wave processes, but some may also be due to instabilities caused by the interactions between the jet stream and other terrain-induced flow distortions (e.g., Clark et al. 2000). Of course, some of these turbulence encounters may be due to jet streams, upper-level fronts, or convective processes that might have occurred in the absence of terrain, but it is assumed that such encounters make only a secondary contribution to the statistics in the vicinity of the steep Greenland topography.

### *a. Monthly turbulence occurrence*

The occurrence of MOG AIREPS is not uniformly distributed throughout the year. Figure 2 shows the monthly distribution of the MOG reports, as well as the number of individual days with at least one MOG report. This figure shows that there are more MOG reports in the winter months than in the summer months. January has the most reports (245, 16% of all MOG reports) in the 7-yr period, and May has the least (54, 3.6% of all MOG reports). Similarly, January has the most days with at least one MOG report (i.e., 86), and May has the least (i.e., 32). Figure 2 does not take into account changes in air traffic through the region of

[1] The definition of MOG used here is different from that used by Wolff and Sharman (2008), which was TB $\geq$ 3.

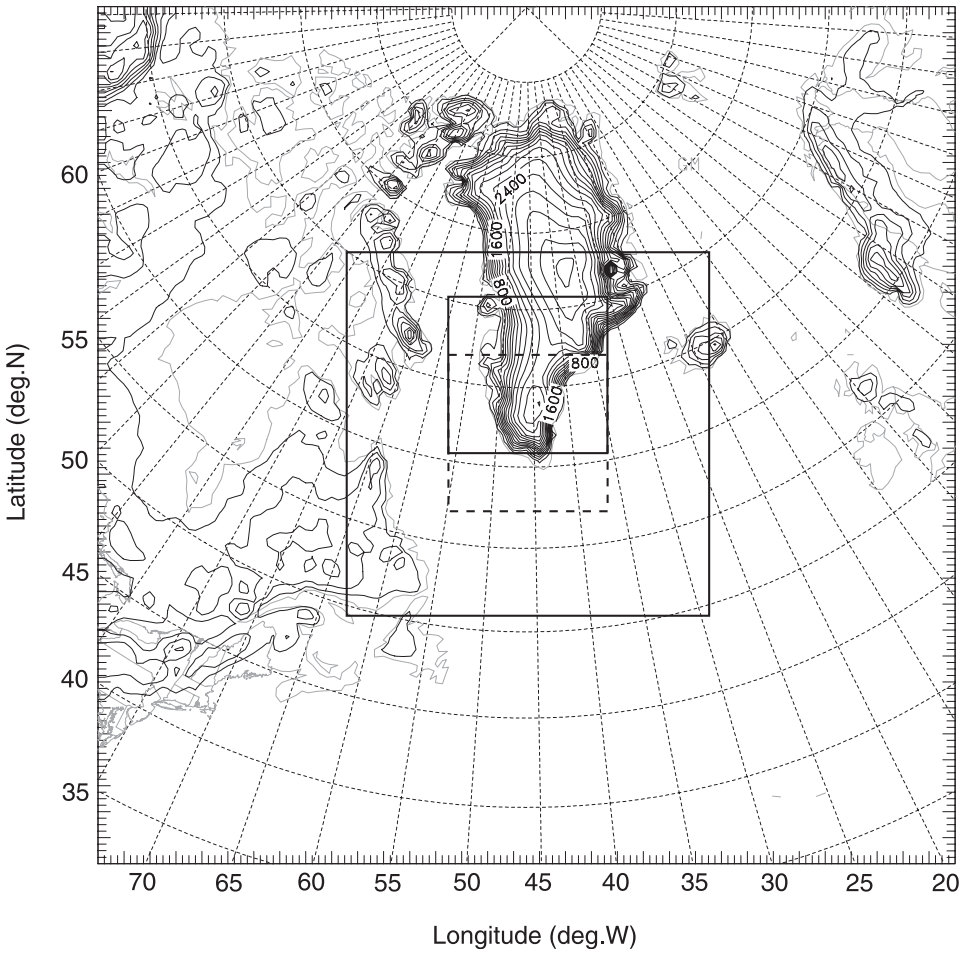


FIG. 1. Terrain elevation (contoured at 200-m intervals). The area shown is the horizontal extent of domain 1 in the COAMPS simulations; also shown is the location of domain 2 and the innermost domain used for the 19 Feb 2000 simulation (solid) and the 11 Jan 2003 simulation (dashed).

interest. The number of commercial flights and their flight tracks are extremely difficult to ascertain from the available data. However, normalizing the number of MOG reports by the total number of reports (including null turbulence) is one way to reduce the influence of spatial and temporal variations in air traffic density (Wolff and Sharman 2008). This normalization is also shown in Fig. 2 and the seasonal distribution is mostly unchanged and reflects a maximum in MOG turbulence occurrence in the winter months and a minimum turbulence occurrence in the summer months. This is a similar distribution to that found for mountain-wave turbulence reports over the contiguous United States by Wolff and Sharman (2008).

The seasonal distribution in turbulence reports can be partially explained by the seasonal variation in the intensity of the jet stream. In the winter months, the meridional temperature gradient is strongest, leading to more intense jets. While the turbulence over Greenland [and over the Rocky Mountains in Wolff and Sharman (2008)] is mainly caused by the presence of mountain waves, stronger jets will lead to increased wind shears, a lower Richardson number, and a higher likelihood of wave instability processes. Moreover, the seasonal distribution of turbulence encounters over Greenland is also strongly coupled to the seasonal variation in surface cyclone occurrence as will be discussed in section 2c and later in the paper.

### *b. Low-level wind direction during turbulent events*

As a simple attempt to delineate the flow regimes responsible for generating turbulence over Greenland, the low-level wind direction is examined for every day with at least one MOG turbulence report during the 7-yr period considered. The wind direction was obtained from the National Centers for Environmental Prediction–National Center for Atmospheric Research (NCEP–NCAR) reanalysis (Kalnay et al. 1996) and to reduce

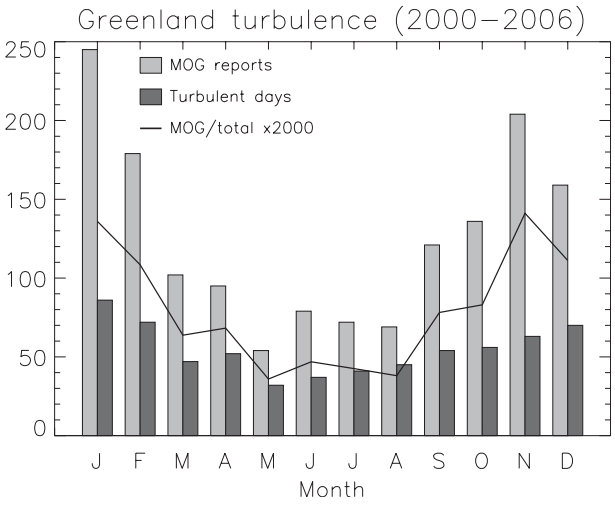


FIG. 2. Monthly distribution of turbulence reports from 2000 to 2006. Shown are the number of MOG turbulence reports (light bar), the number of days with at least one MOG report (dark bar), and the number of MOG reports divided by the total number of turbulence reports (null–extreme) in that given month (multiplied by 2000, solid line).

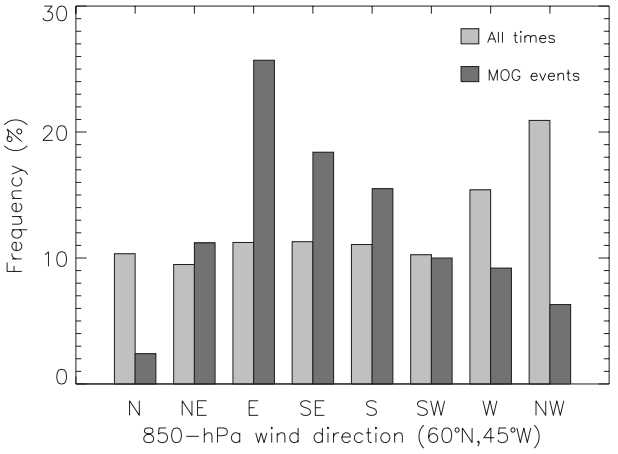


FIG. 3. Distribution of 850-hPa wind directions at 60°N, 45°W derived from the NCEP–NCAR reanalysis between 2000 and 2006. Shown is the distribution determined from the 6-hourly data (light bar), and those wind directions occurring during turbulent events (dark bar).

the influence of low-level blocking the 850-hPa winds were used. To further reduce the uncertainty in this analysis associated with spatial changes in wind direction, our focus is restricted to MOG reports in the vicinity of Greenland's southern tip. In the event that a MOG report occurred within latitudes between 59° and 70°N and longitudes between 35° and 60°W, the wind direction at the approximate location of Greenland's southern tip (65°N, 45°W) was recorded.

The distribution of the 850-hPa wind direction on turbulent days is shown in Fig. 3. Also shown in Fig. 3 for comparison purposes is the distribution of the 850-hPa wind direction at (65°N, 45°W) for every day during the 7-yr period. Therefore, while the wind at Greenland's southern tip is most commonly from the west or northwest, approximately 60% of the turbulent events occur when the low-level wind is from the southeast quadrant; turbulence is disproportionately more likely in easterly, southeasterly, or southerly flow regimes. Furthermore, when the low-level wind is from the northwest quadrant, turbulence is less frequent and only accounts for approximately 18% of the turbulence events.

To explore the flow regimes when the turbulence is more intense or widespread, a number of *significant events* were identified. The criterion for identifying these significant events was 1) at least one report of severe or greater turbulence, or 2) at least 10 MOG reports during any one day. Using this criterion, 43 significant events were identified, which corresponds to about 6.5% of all days with at least 1 MOG report. Of these significant events, 19 have low-level winds from the east or southeast (44% of all significant events). Consistent with the distribution shown in Fig. 2, 18 of these significant events occurred between September and November, 17 occurred between December and February, 6 occurred between March and May, and only 2 of these significant events occurred between June and August.

### c. *Interpretation of turbulence statistics*

Sections 2a,b highlighted two important aspects of the temporal variability of MOG turbulence encounters over Greenland: (i) turbulence is more likely to occur when the low-level wind is from the southeast quadrant; and (ii) turbulence is more frequent during the winter months. One potential source of low-level southeasterly flow is the passage of cyclones across the southern reaches of Greenland. Seasonal variations in the large-scale circulation (viz., storm tracks) will modify the frequency of occurrence of cyclones. Such variations coupled with the importance of low-level southeasterly flow likely contribute to the seasonal variations in turbulence occurrence shown in Fig. 2.

The climatological frequency of cyclones was assessed using the University of Melbourne automated cyclone tracking scheme (Murray and Simmonds 1991). This scheme identifies regions of surface pressure minima (viz., cyclones) from gridded data and determines a variety of relevant statistics including location, frequency of occurrence, intensity, and track. The *cyclone density* was determined for the 2000–06 period for the summer [June–August (JJA)] and winter [December–February (DJF)] months separately using the NCEP–NCAR reanalysis database, where cyclone density is a

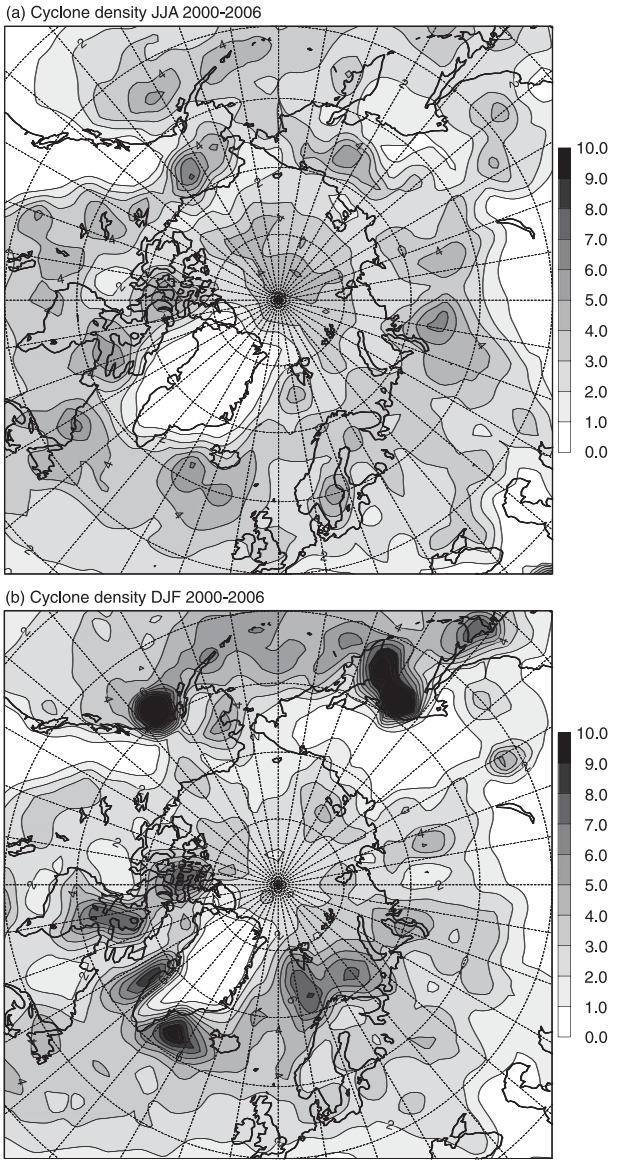


FIG. 4. Cyclone density [$\times 10^{-3}$/(° latitude)$^2$] derived from the NCEP–NCAR reanalysis between 2000 and 2006: (a) JJA and (b) DJF.

measure of the frequency of occurrence of cyclones. Figure 4 illustrates that there are approximately 2–3 times more cyclones in DJF than in JJA in the vicinity of Greenland's southern tip.

When flow is incident upon Greenland's southern tip mountain waves may be generated and propagate vertically until they become evanescent or are dissipated at a critical level. Such generation and propagation conditions will vary significantly case by case, yet the flow regime associated with the passage of surface cyclones presents a simple scenario that is consistent among many cases. Consider a surface cyclone whose center passes over the southern tip of Greenland: this cyclone directs low-level southeasterly flow over the terrain, which generates mountain waves that may propagate vertically.[2] However, as is common, the upper-level flow maintains a westerly component. Therefore, the presence of the surface low suggests that a change in wind direction of at least 90° is likely, presenting a scenario that is conducive to the presence of a critical level, as defined in the introduction. An example of this scenario is shown in Fig. 5, based on one significant turbulence event (19 February 2000) described in more detail later in the paper.

The described scenario, relating the presence of a surface cyclone to the generation of turbulence aloft, requires a number of processes to be present. First, the incident conditions must be conducive to the generation of vertically propagating mountain waves. For example, the parameter $Nh/U$, where $N$ is the Brunt–Väisälä frequency, $U$ is the wind speed, and $h$ is the terrain height, must not be too large; in flow regimes with large values of $Nh/U$, the incident flow is more likely to be blocked and deflected. Second, for this process to influence commercial aviation the change in wind direction must exceed a significant angle, and the height of this change must be at the appropriate altitude. These two processes were examined for each of the 19 significant events with easterly or southeasterly low-level wind described in the section 2b.

To determine the presence of mountain waves, Advanced Very High Resolution Radiometer (AVHRR) infrared (IR) satellite images were examined for evidence of mountain-wave signatures in the cloud field (e.g., a *föhn gap* or similar feature); Fig. 5c shows one example for 19 February 2000 with the extent of the föhn gap highlighted by arrows. Satellite imagery for each of the significant events was examined, and 17 of the 19 cases (89%) with easterly or southeasterly low-level wind showed evidence of mountain waves. The winds from the NCEP–NCAR reanalysis were also examined for each of these 19 significant events. Of those 19, 17 exhibited at least a 90° shift in the wind direction below 100 hPa. Therefore, it is apparent from the cursory examination of the large-scale conditions and MOG turbulence reports, that an important regime contributing to the generation of turbulence near Greenland is associated with the passage of cyclones. It is beyond the scope of this study to examine each turbulence event in any significant detail, and the remainder of this study is

[2] While the vertical group velocity of mountain waves varies with background conditions, it is likely that waves would span the depth of the troposphere within a few hours of the onset of cross-mountain flow.

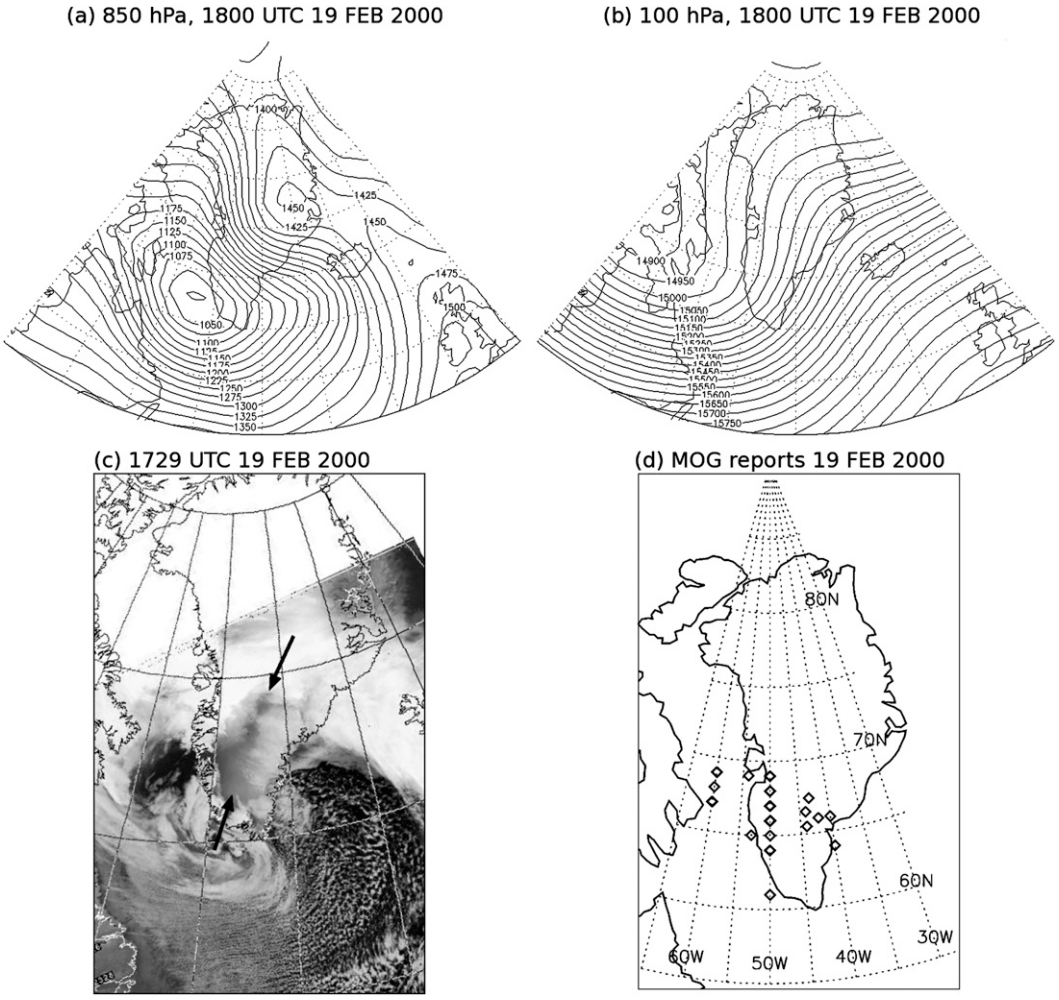


FIG. 5. The (a) 850- and (b) 100-hPa geopotential height (m) from the NCEP–NCAR reanalysis at 1800 UTC 19 Feb 2000, (c) AVHRR IR (11.5–12.5 $\mu$m) image valid at 1729 UTC, and (d) the horizontal location of the MOG turbulence reports for this day (the altitude, location, and severity of these reports are listed in Table 1). Arrows in (c) highlight signatures of mountain waves.

dedicated to examining two cases that are consistent with the proposed scenario.

## 3. Numerical simulations

This section presents two of the significant events selected for further examination using the atmospheric portion of the Coupled Ocean–Atmosphere Mesoscale Prediction System (COAMPS; Hodur 1997). The COAMPS atmospheric model is a finite-difference approximation to the fully compressible, nonhydrostatic equations. Physical parameterizations are used to represent surface fluxes, boundary layer, radiation, and moist processes including microphysical quantities (see Hodur 1997). The initial fields for the model are created from multivariate optimum interpolation analyses of upper-air sounding, surface, commercial aircraft, and satellite data that are quality controlled. The lateral boundary conditions for the outermost mesh make use of Navy Operational Global Analysis and Prediction System (NOGAPS) forecast fields. The model is initialized at 0000 UTC on the day of interest. COAMPS has been verified with field campaign datasets on numerous occasions to demonstrate reasonable skill in simulating topographically forced flows such as mountain waves (e.g., Doyle et al. 2005; Doyle and Jiang 2006).

The model was configured with three (one way) nested domains with horizontal grid spacing equal to 45, 15, and 5 km, and 60 vertical levels. The location of these three domains is illustrated in Fig. 1; both simulations described in this paper use the same configurations, with the exception of the location of the highest-resolution domain.

TABLE 1. List of all MOG reports on 19 Feb 2000. (Note the altitude of flight is determined using standard atmospheric pressure levels and the physical height above sea level varies with the conditions. Nevertheless, 30 000 ft is approximately 9.8 km, 35 000 ft is approximately 11.5 km, and 40 000 ft is approximately 13.1 km.)

| Time (UTC) | Lat (°N) | Lon (°W) | Flight level (ft) | Turbulence |
|---|---|---|---|---|
| 724 | 68 | 50 | 33 000 | 4 |
| 846 | 61 | 50 | 37 000 | 8 |
| 918 | 61 | 50 | 37 000 | 5 |
| 949 | 67 | 50 | 37 000 | 6 |
| 1336 | 64 | 40 | 37 000 | 4 |
| 1354 | 66 | 42 | 33 000 | 4 |
| 1408 | 64 | 50 | 37 000 | 4 |
| 1413 | 65 | 50 | 29 000 | 5 |
| 1420 | 66 | 40 | 35 000 | 5 |
| 1449 | 66 | 50 | 35 000 | 5 |
| 1502 | 69 | 54 | 33 000 | 5 |
| 1521 | 65 | 53 | 33 000 | 5 |
| 1526 | 65.5 | 44 | 28 000 | 4 |
| 1544 | 66 | 50 | 27 000 | 4 |
| 1558 | 69 | 60 | 33 000 | 4 |
| 1616 | 64 | 50 | 33 000 | 5 |
| 1616 | 67 | 50 | 37 000 | 4 |
| 1642 | 67 | 60 | 35 000 | 4 |
| 1708 | 66.5 | 44 | 31 000 | 5 |
| 1709 | 66 | 50 | 35 000 | 4 |
| 1752 | 67.4 | 43.22 | 26 000 | 5 |
| 1752 | 67 | 60 | 31 000 | 4 |
| 1806 | 68 | 60 | 28 000 | 4 |
| 1829 | 69 | 50 | 35 000 | 5 |
| 1851 | 66 | 50 | 35 000 | 4 |
| 1851 | 66 | 50 | 35 000 | 4 |
| 1943 | 66 | 50 | 39 000 | 4 |
| 2028 | 67 | 50 | 34 000 | 4 |
| 2033 | 68 | 50 | 37 000 | 4 |
| 2039 | 69 | 50 | 32 000 | 4 |
| 2104 | 69 | 60 | 33 000 | 4 |
| 2119 | 67 | 50 | 35 000 | 5 |
| 2147 | 67 | 60 | 35 000 | 4 |

### *a. 19 February 2000*

On 19 February 2000 there were 33 MOG reports of turbulence in the vicinity of Greenland, including one severe report and one extreme report (Table 1). The location of these reports is shown in Fig. 5d. As discussed in the previous section (Figs. 5a–c), this case features an eastward-moving surface cyclone, low-level (850 hPa) southeasterly winds, upper-level (100 hPa) west-southwesterly winds, evidence of mountain-wave activity from satellite imagery, and is therefore a good candidate for turbulence formation by three-dimensional critical level processes. Although the extreme turbulence report was made at 0846 UTC, our discussion is restricted to late afternoon when the majority of the turbulence was reported.

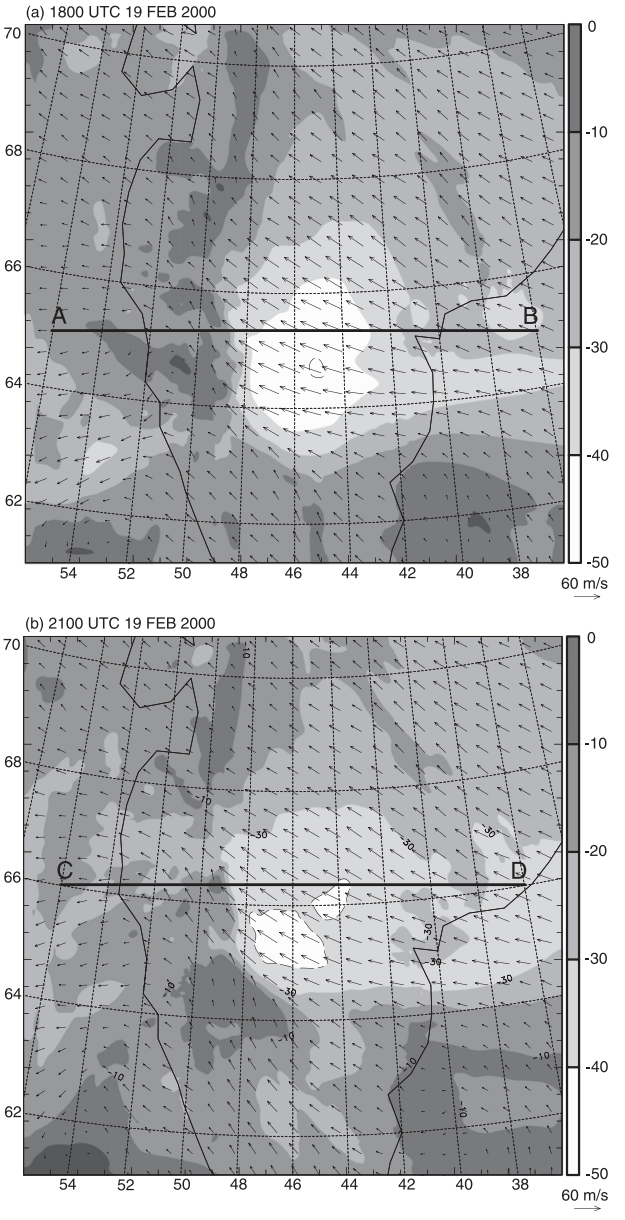


FIG. 6. Horizontal cross section at 500 hPa from COAMPS domain 3 at (a) 1800 and (b) 2100 UTC 19 Feb 2000. Wind vectors represent the horizontal wind speed and direction, and shading depicts the zonal wind. Also shown are the locations of cross sections used in Figs. 7 and 8 (lines AB and CD); these cross sections are at different latitudes.

The COAMPS simulation, for this situation, shows that accompanying the eastward progression of the surface cyclone is a midlevel (500 hPa) east-southeasterly jet that moves toward the north as time continues (Fig. 6) and contains wind speeds exceeding 40 m $s^{-1}$. Zonal cross sections of the zonal velocity (Fig. 7) illustrate that the flow maintains an easterly component until approximately 13-km altitude, where the flow reverses to a

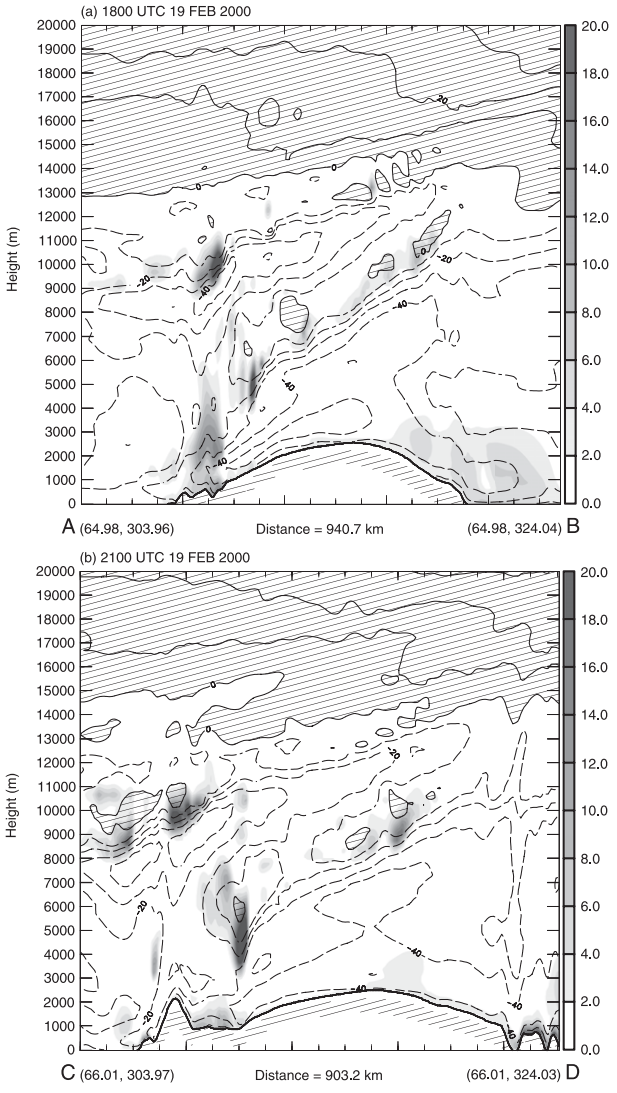


FIG. 7. Zonal cross section at (a) 1800 (line AB from Fig. 6a) and (b) 2100 UTC (line CD from Fig. 6b) 19 Feb 2000 from the COAMPS simulation. Contours show zonal wind at 10 m $s^{-1}$ intervals, with negative contours dashed, and regions of positive wind hatched. Also shown is subgrid TKE ($m^2$ $s^{-2}$; shaded).

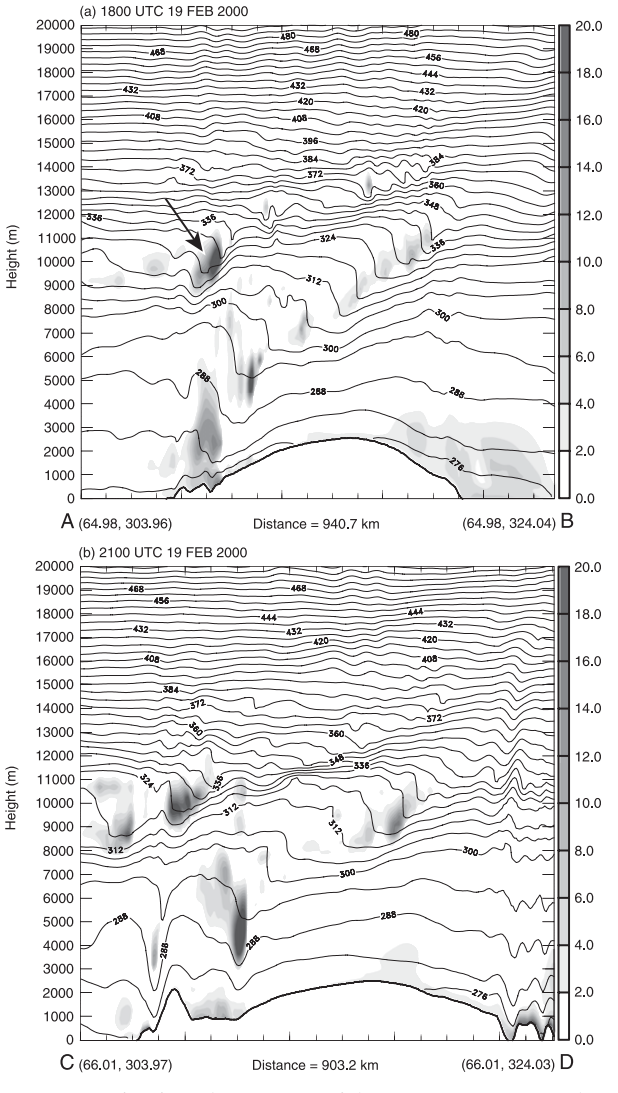


FIG. 8. As in Fig. 7, but for potential temperature contoured at 6-K intervals. A region of turbulence discussed in the text is highlighted in (a) with an arrow.

westerly direction. Within the easterly flow are localized regions of flow reversal (westerly flow) that are located within coherent shear zones; these shear zones have features consistent with upward-propagating mountain waves (i.e., backward phase tilt with height). These regions of tropospheric flow reversal all contain nonzero parameterized turbulent kinetic energy (TKE), identifying regions of instability. Consistent with the regions of localized TKE are wave-induced regions of reduced stability (Fig. 8), resembling hydraulic jump–like features.

The simulation suggests that there are two important processes apparently at play. The first process is the steepening of the large-scale vertically propagating mountain wave, associated with the tilted phase structure that extends across the width of the Greenland landmass. This steepening and eventual instability occurs over a region of positive (backward) wind shear, a few kilometers below the (zonal) flow reversal. The second process is the steepening of small-scale gravity waves associated with localized features in the terrain. Both the southern (line AB) and northern (line CD) cross sections highlight localized regions of instability above Greenland's western slopes. Figure 8a illustrates enhanced low-level TKE above the multiple (small) peaks, with additional instability at around 11 km, which is highlighted by an arrow on the figure. Furthermore, Fig. 8b identifies the localized steepening and instability at 11 km, directly linked to the flow down the relatively

steep lee slope of the isolated peak at the western edge of Greenland. Both regions of wave breakdown occur about two kilometers below the reversal in the zonal flow at 13 km, likely because of nonlinearity associated with wave reflection at the mean critical level and the subsequent resonance. Moreover, the wind shear is relatively weak in the lower stratosphere, allowing nonlinear effects to induce local regions of *wave-induced criticality* some distance below the critical level defined by the background flow. The altitude of the simulated TKE is consistent with those reports detailed in Table 1 and, notwithstanding the uncertainties in horizontal location, consistent with the preference for reports at 50°W. Specifically, three moderate turbulence reports were recorded within 1 h and 1° latitude or longitude of the region of turbulence highlighted in Fig. 8a (see Table 1). Furthermore, the northward movement of the midlevel easterly jet is consistent with the northward progression of MOG turbulence reports as time continues throughout 19 February 2000: ranging from the extreme report at 0846 UTC at 61°N to the numerous reports between 67° and 69°N around 2100 UTC.

### *b. 11 January 2003*

The 11 January 2003 case shows many similarities to the 19 February 2000 case. The 11 January 2003 turbulence reports are listed in Table 2. There are 36 MOG reports in total, making it the leading significant case in the 7-yr database. Of these 36 MOG reports, 4 were in the moderate-to-severe category and 3 were severe reports. The large-scale conditions for this event are depicted in Fig. 9, along with an AVHRR satellite image, and the spatial locations of all of the MOG turbulence reports. In a similar fashion to 19 February 2000, the 11 January 2003 case is characterized by low-level (850 hPa) southeasterly flow directed over the southern tip of Greenland. However, in this case, the low pressure system is larger and the minimum surface pressure resides to the west of Greenland. The wind rotates with altitude, and by 100 hPa the wind at Greenland's southern tip is westerly. The satellite image shows a well-defined mountain-wave signature (Fig. 9c), highlighted in the figure by arrows. Thus, this case fits within the previously discussed archetype, with the possibility of mountain-wave–critical level interactions due to directional wind shear.

The turbulence reports on 11 January (Table 2) are generally situated farther south than on 19 February 2000 and for this reason, the COAMPS simulation of 11 January (Figs. 10–12) uses a 5-km domain that is 2° latitude farther to the south in comparison to the previous case. The 500-hPa wind is easterly over a significant area above Greenland (Fig. 10). At 1200 UTC (Fig. 10a), the 500-hPa wind exhibits significant mesoscale structure, with strong horizontal shear evident at approximately 61°N, 45°W to the south of a strong easterly jet with strength exceeding 40 m $s^{-1}$. Also, there is a south–north-oriented band of horizontal shear at 48°W that extends from 61° to 65°N. As time continues (Fig. 10b), this easterly jet moves poleward, and the mesoscale detail in the horizontal flow is still present but less striking.

Zonal cross sections of the zonal velocity (Fig. 11), illustrate that the (zonal) flow reversal resides at higher altitudes than the previous case, with the background critical level at about 15 km. Nonetheless, localized regions of enhanced TKE exist at around 11 km. While at both times the wind shows evidence of large-scale phase tilt in the zonal wind, it is unlike the 19 February case that showed descent of the westerly flow in the large-scale mountain-wave signatures. In this case, localized

TABLE 2. List of all MOG reports for 11 Jan 2003.

| Time (UTC) | Lat (°N) | Lon (°W) | Flight level (ft) | Turbulence |
|---|---|---|---|---|
| 0525 | 60 | 50 | 32 000 | 5 |
| 1203 | 61 | 50 | 36 000 | 4 |
| 1209 | 61 | 50 | 36 000 | 4 |
| 1326 | 63 | 50 | 35 000 | 4 |
| 1330 | 61 | 50 | 37 000 | 4 |
| 1356 | 63 | 46 | 32 000 | 5 |
| 1401 | 62 | 50 | 33 000 | 4 |
| 1406 | 63 | 50 | 35 000 | 5 |
| 1407 | 64 | 50 | 36 000 | 4 |
| 1409 | 63 | 50 | 34 000 | 4 |
| 1412 | 61 | 50 | 32 000 | 4 |
| 1425 | 62 | 50 | 32 000 | 5 |
| 1429 | 63 | 50 | 37 000 | 4 |
| 1445 | 62 | 45 | 33 000 | 4 |
| 1505 | 62 | 50 | 33 000 | 4 |
| 1535 | 63 | 50 | 35 000 | 4 |
| 1542 | 65 | 50 | 39 000 | 4 |
| 1559 | 62 | 50 | 33 000 | 4 |
| 1559 | 62 | 50 | 33 000 | 4 |
| 1635 | 63 | 50 | 37 000 | 4 |
| 1635 | 61 | 48 | 30 000 | 4 |
| 1637 | 61 | 48 | 30 000 | 4 |
| 1653 | 63 | 50 | 37 000 | 4 |
| 1657 | 63 | 50 | 30 000 | 4 |
| 1701 | 63 | 50 | 31 000 | 4 |
| 1712 | 63.85 | 52 | 35 000 | 6 |
| 1828 | 64 | 50 | 32 000 | 4 |
| 1909 | 65 | 50 | 34 000 | 4 |
| 1926 | 63 | 50 | 35 000 | 4 |
| 1946 | 64 | 50 | 35 000 | 6 |
| 1947 | 62 | 50 | 32 000 | 4 |
| 2052 | 65 | 50 | 36 000 | 4 |
| 2107 | 63 | 50 | 33 000 | 4 |
| 2116 | 63 | 50 | 33 000 | 6 |
| 2148 | 65 | 30 | 34 000 | 4 |
| 2250 | 63 | 50 | 34 000 | 4 |

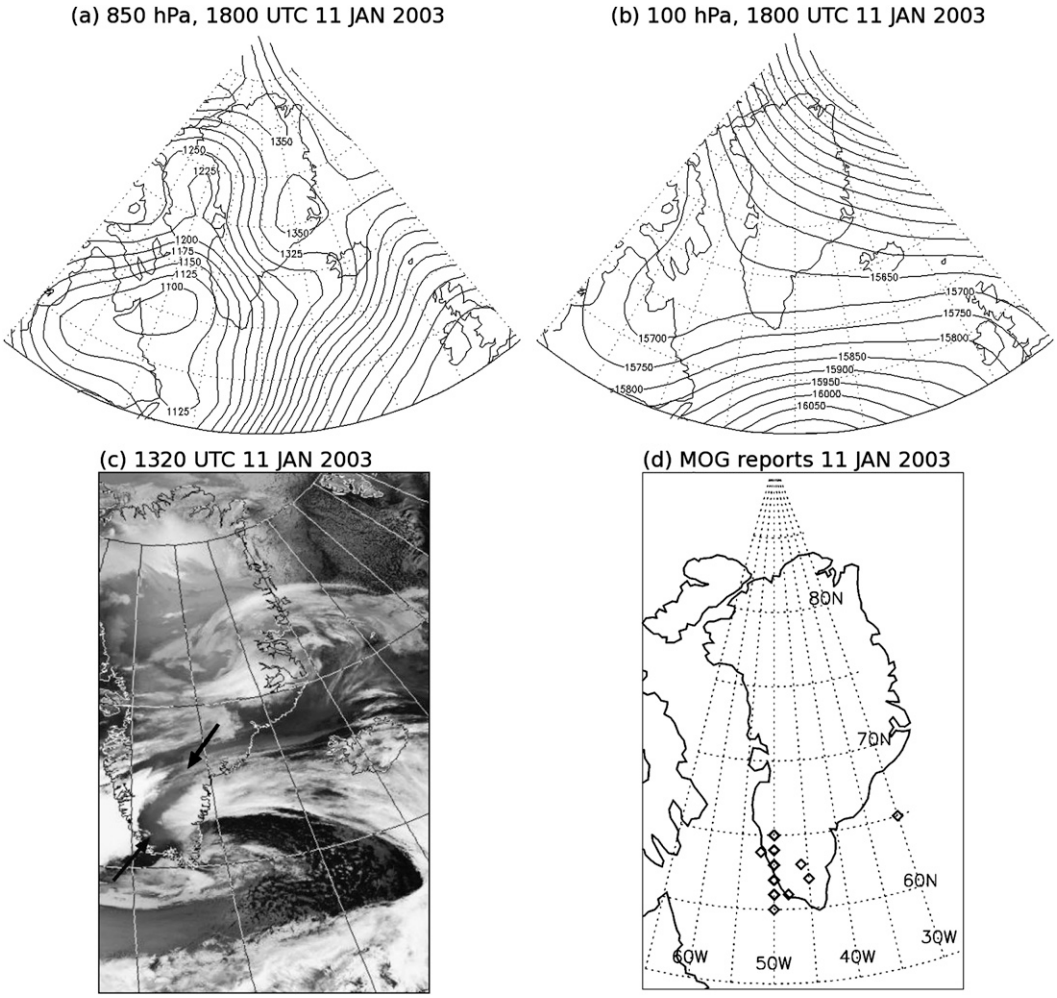


FIG. 9. As in Fig. 5, but for 11 Jan 2003 and (c) is valid at 1320 UTC. The altitude, location, and severity of the reports shown in (d) are listed in Table 2.

regions of wave-induced flow reversal occur at low levels near the lee slope and at a region of apparent wave breaking at 10–11 km directly above that lee slope; this region of localized flow reversal is particularly evident at 1800 UTC (Fig. 11b).

The potential temperature distribution (Fig. 12) elucidates the important differences between 11 January 2003 and the 19 February 2000 case. On 11 January, at both cross sections (and times) the mountain-wave response above the lee slope is highly nonlinear. The wave response is dramatic, appearing similar to a deep hydraulic jump, with peak-to-peak amplitude of approximately 5 km. This large-amplitude response induces enhanced TKE at low altitudes, as well as highly localized overturning just below the tropopause. At the southernmost cross section (Fig. 12a, line GH) the TKE is strongest at lower altitudes, while in the northernmost cross section (Fig. 12b, line EF) the TKE is largest in the localized overturning region just below the tropopause, which is highlighted by an arrow in the figure. [Note that one severe and two moderate turbulence reports were recorded within 1 h and approximately 1° latitude or longitude of this location (see Table 2).] This highlighted region of upper-level turbulence is likely associated with resonance linked to wave reflection by the mean critical level farther aloft and partial wave reflection at the tropopause, which both act to amplify the wave signal to the point that a wave-induced critical level is produced many kilometers below the mean critical level. This mechanism is similar in concept to that described by Clark and Peltier (1984).

The two cases show many similarities, but certainly differ in detail. In particular, the 11 January case shows a large-amplitude wave response in the lower troposphere, whereas the 19 February wave response is relatively modest. Comparison of Figs. 7 and 8 with Figs. 11

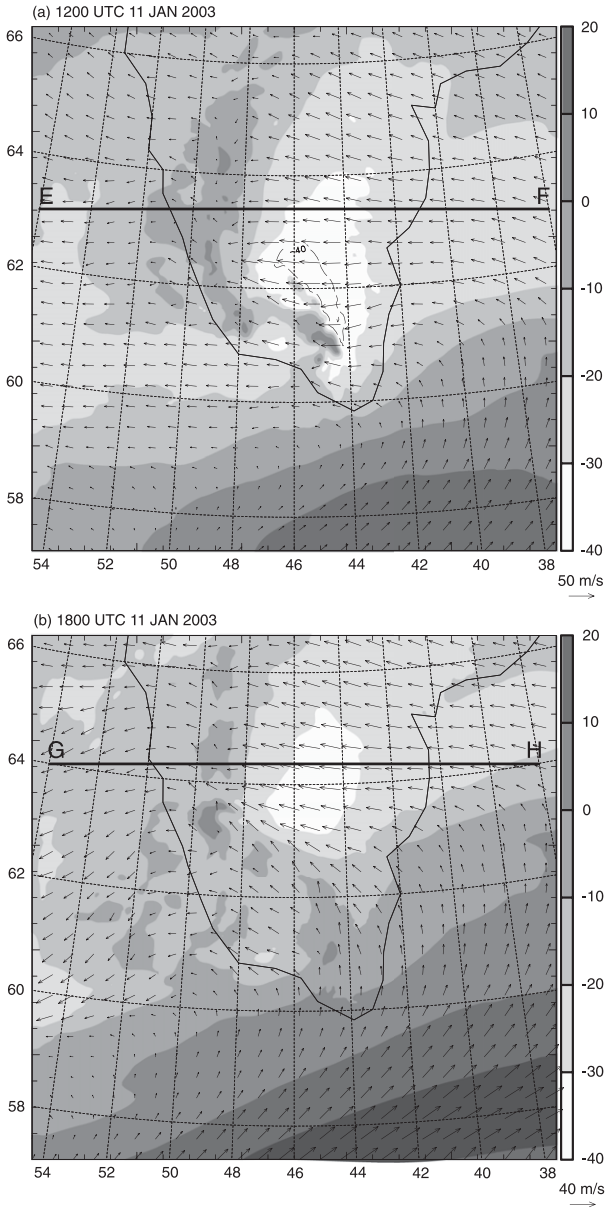


FIG. 10. Horizontal cross section at 500 hPa from COAMPS domain 3 at (a) 1200 and (b) 1800 UTC 11 Jan 2003. Wind vectors represent the horizontal wind speed and direction, and shading depicts the zonal wind. Also shown are the locations of cross sections used in Figs. 11 and 12 (lines EF and GH; these cross sections are at different latitudes).

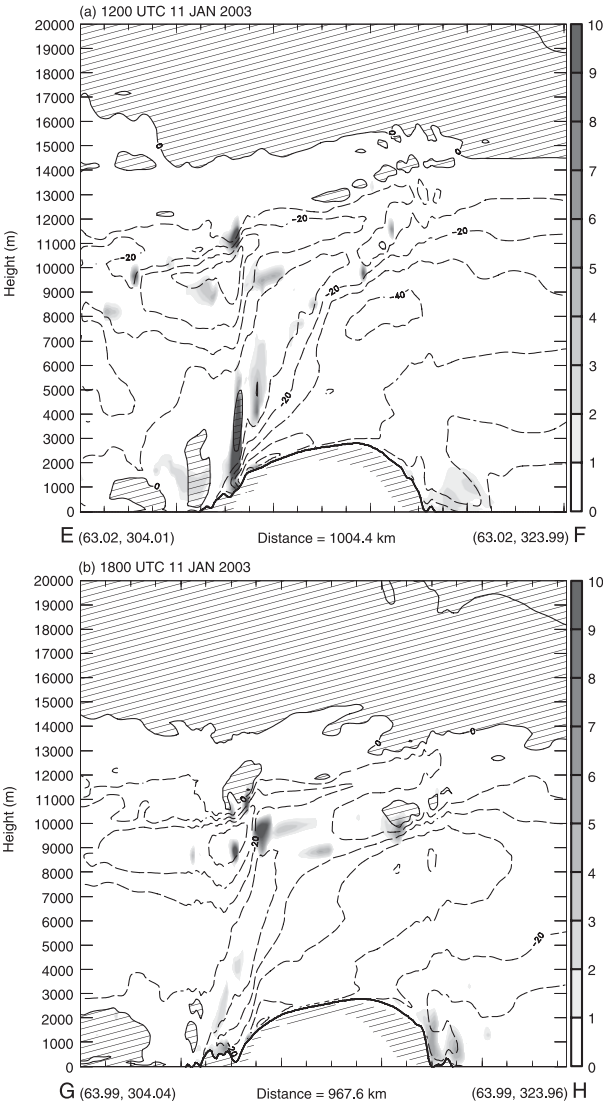


FIG. 11. As in Fig. 7, but at (a) 1200 UTC (line EF from Fig. 10a) and (b) 1800 UTC (line GH from Fig. 10b) 11 Jan 2003.

and 12 show that the two events have similar upstream stability structure, with the mean tropospheric Brunt–Väisälä frequency approximately 0.008 $s^{-1}$. The principal difference, however, is in the low-level wind speed: the 19 February case has a low-level upstream zonal wind of approximately $-40$ m $s^{-1}$, whereas the 11 January case has a low-level zonal wind of approximately $-20$ m $s^{-1}$. Using $h = 3000$ m, the $Nh/U$ parameter is equal to 0.6 on 19 February and 1.2 on 11 January. As originally shown mathematically in two dimensions by Miles in a series of papers (e.g., Miles and Huppert 1968) and in three dimensions using numerical simulation (e.g., Smolarkiewicz and Rotunno 1989), $Nh/U$ can be interpreted as a measure of nonlinearity of the flow. The increased amplitude in the low-level wave response on 11 January is consistent with an increase in $Nh/U$ and also consistent with the idealized results of Smolarkiewicz and Rotunno (see their Figs. 3a,b).

## 4. Discussion relevant to aviation safety

The two turbulence events and associated mountain-wave structures described in section 3 represent the two

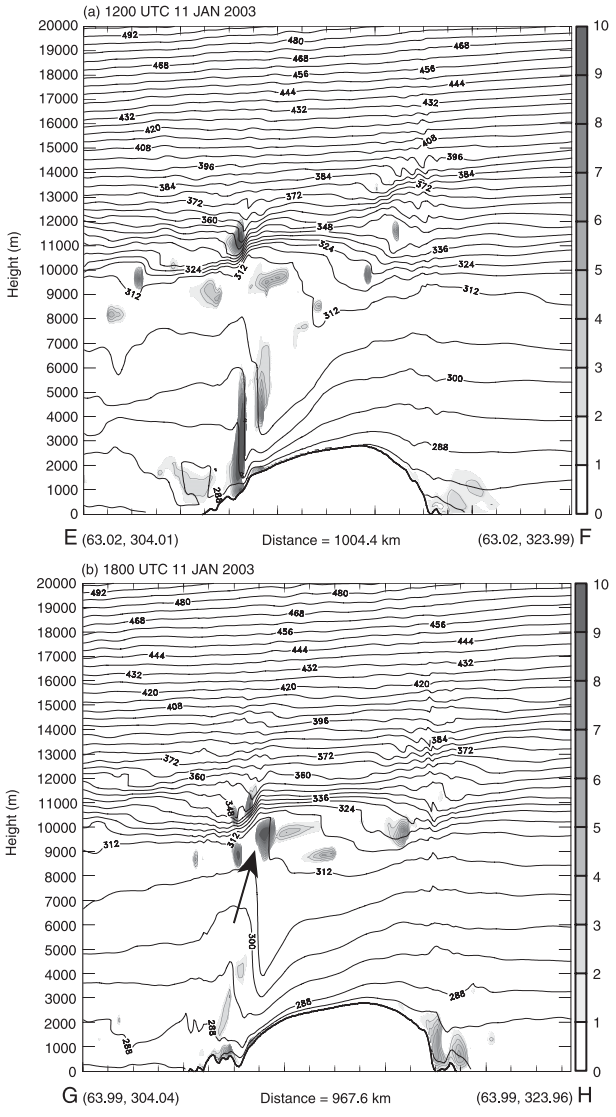


FIG. 12. As in Fig. 11, but for potential temperature contoured at 6-K intervals. (b) A region of turbulence discussed in the text is highlighted with an arrow.

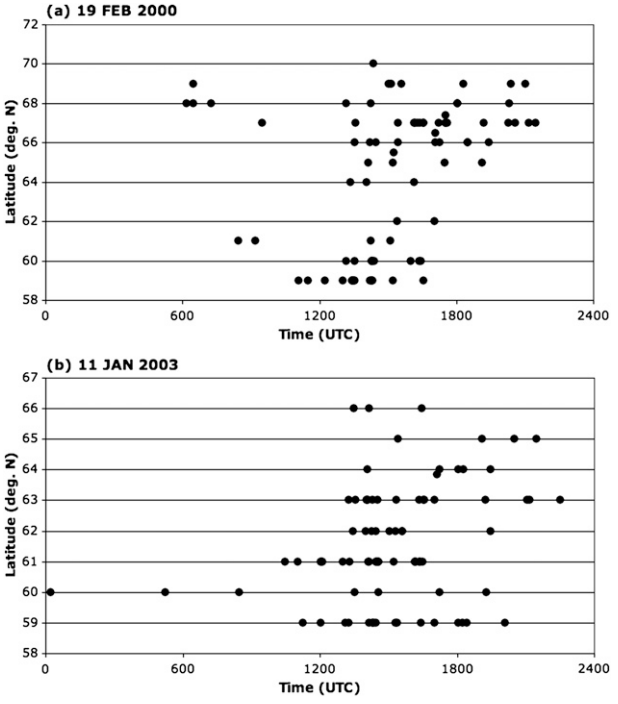


FIG. 13. The latitude of all turbulence reports in our area of interest vs time (UTC) for (a) 19 Feb 2000 and (b) 11 Jan 2003.

most significant days in our 7-yr database, with ''significance'' quantified in terms of the number of MOG turbulence reports. This measure is, however, somewhat subjective and related to a variety of factors including the volume of air traffic, the altitude of flight, the location of the flight path, and some element of randomness. The location of the flight route in the north–south direction seems particularly important; these flight routes will change throughout the day, presumably based on optimum wind conditions, and prior locations of turbulence occurrence (and null occurrence). For example, consider the latitude of all turbulence reports (including null) versus time on 19 February 2000 and 11 January 2003 (Fig. 13). Both days show a tendency for more reports farther to the north later in the day. Moreover, 19 February (Fig. 13a) shows a distinct bimodal distribution, implying two distinct flight routes, with the southernmost route being ''closed'' at around 1700 UTC. Both days also show a similar northward trend in the number of MOG reports as the day progresses (see Tables 1 and 2). This northward progression of the MOG reports may simply be indicating a northward movement of the flight tracks during the day and may not be related to meteorological processes. However, both COAMPS simulations indicate enhanced turbulence farther to the north during the northward progression of the midlevel (500 hPa) easterly jet. Therefore, the model results suggest that on these days a northward movement of flight tracks would likely place aircraft in the least favorable location.

The uncertainties associated with the AIREP data lead to limitations in the assessment of cases where this specific flow regime does not generate turbulence. For instance, it is possible to identify other days that have the same flow regime, but do not have turbulence reports; 26 August 2001 is one such day and the large-scale synoptic wind conditions represent what appears to be the quintessential example of this flow regime (Figs. 14a,b). While not as well defined as the previous two cases, the satellite image shows a weak signature of mountain-wave activity in the cloud field (Fig. 14c,

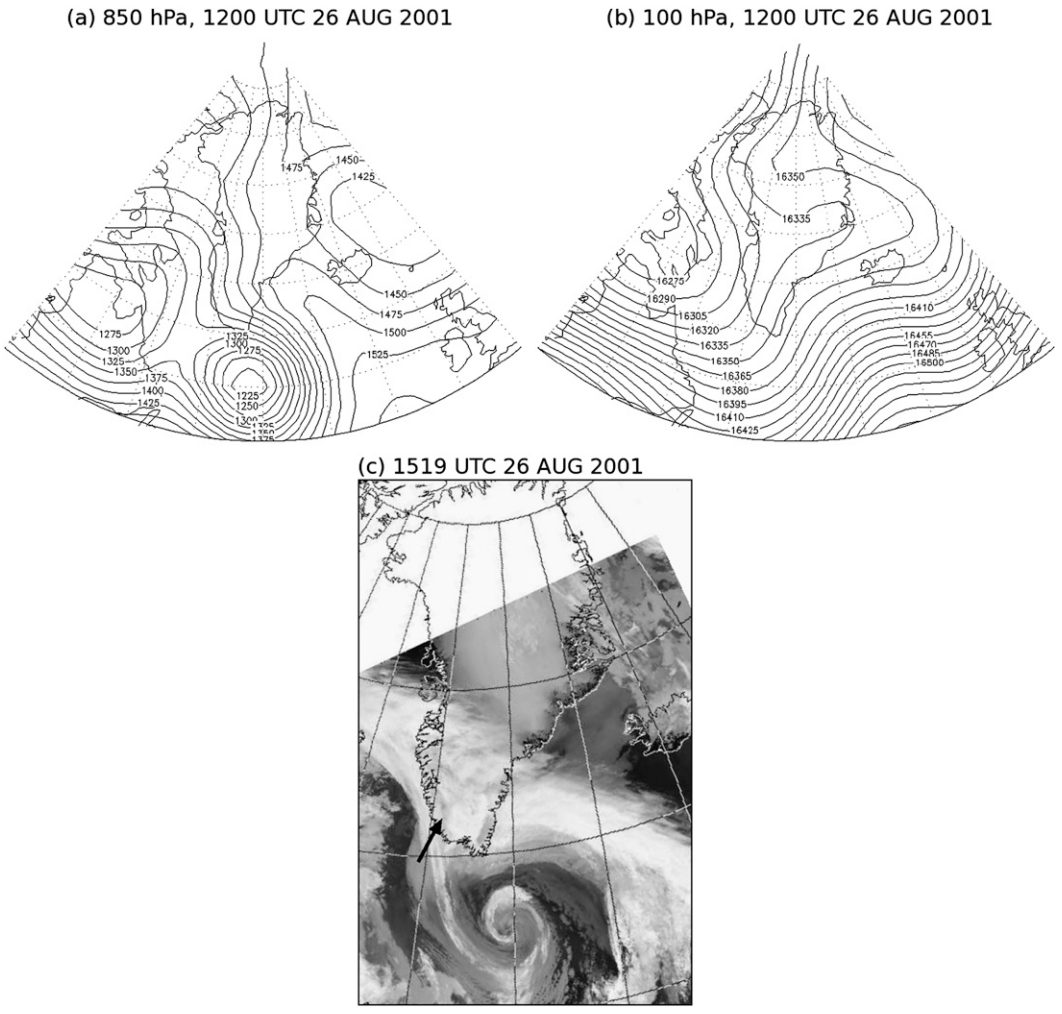


FIG. 14. Geopotential height (m) at (a) 850 and (b) 100 hPa from the NCEP–NCAR reanalysis at 1200 UTC 26 Aug 2001. (c) AVHRR IR image valid at 1519 UTC. The arrow in (c) highlights signatures of mountain waves.

marked by an arrow). This day, however, featured only null turbulence reports (a total of 39) in our area of interest. Nevertheless, of these 39 null reports, 29 of them were over the ocean just to the south of Greenland ($\leq$60°N), and fell outside the region of expected mountain-wave activity. The mountain waves may have been too weak on this (summer) day to generate widespread turbulence, consistent with the seasonal distribution in turbulence encounters depicted in Fig. 2. However, this day may simply be one example of the choice of flight tracks being beneficial in avoiding turbulence, whether by luck or design.

## 5. Summary

This study examined commercial aircraft turbulence reports, meteorological analyses, and numerical simulations in the vicinity of Greenland, identifying processes that contribute to the variability of turbulence encounters. It was shown that turbulence is more common over Greenland during the winter months and more likely to occur when the low-level wind near Greenland's southern tip is from the southeast quadrant. The passage of extratropical cyclones to the south of the turbulent regions is one source of low-level southeasterly flow, and as illustrated using an automated cyclone-tracking scheme, these also influence Greenland's southern tip more commonly in winter than summer.

These results show that a flow regime conducive to wave breaking and turbulence near the southern tip of Greenland occurs during the eastward passage of surface low pressure systems. The resultant incident southeasterly low-level flow may result in the generation of vertically propagating mountain waves. Commonly,

the wind will rotate toward the east with height and these mountain waves can interact with this directional wind shear and break because of three-dimensional critical level interactions. While each case will differ in detail and notwithstanding the contributions from other turbulence sources (e.g., jets, fronts, convection, etc.), the long-term turbulence statistics and the two specific cases examined in more detail herein imply the importance of this mechanism in contributing to the occurrence of enhanced levels of turbulence encounters near Greenland.

Two specific events were examined in more detail using a mesoscale numerical prediction model (i.e., COAMPS). The COAMPS simulations provided realistic simulations of mountain-wave breaking and (parameterized) turbulence at locations consistent with the aircraft turbulence reports. Turbulence was shown to be tied to large-amplitude mountain-wave breaking that occurred a few kilometers below the background critical level. This instability is most likely related to nonlinear processes and wave resonance associated with wave reflection at the background critical level. In these two cases, the wave response associated with the western lee slope of Greenland was the most influential. The simulations also identified the importance of transient wind structures [viz., northward-progressing midtropospheric (500 hPa) jets], which contributed to the temporal variability of turbulence occurrence and intensity. Thus, identifying the presence of these jets may be useful for turbulence avoidance strategies.

This study focused on the flow regime characterized by low-level southeasterly flow and critical-level interactions associated with directional wind shear. This focus arose out of the apparently disproportionate occurrence of turbulence in southeasterly (low level) flow regimes. Somewhat surprisingly, the westerly and northwesterly wind directions were less likely to produce turbulence (reports) than climatology would dictate. The westerly flow regime might be expected to produce the largest wave response (e.g., Doyle et al. 2005), and was shown by Wolff and Sharman (2008) to be the most common scenario over the Rocky Mountains. Doyle et al. did identify wave breaking in the lower stratosphere, but the absence of a critical level in such cases means that the altitude of the upper-level wave breaking is heavily dependent on the wave amplitude, which was shown to be sensitive to a variety of upstream conditions. Thus, it seems reasonable to assume that in many cases of west or northwesterly flow the upper-level wave breaking may occur above the usual flight level of most commercial air carriers (~10 km), leaving lower altitudes relatively free of turbulence. Therefore, the results elucidated by the turbulence statistics herein can only be applied to turbulence near 10 km (i.e., the part of the atmosphere sampled by commercial air travel).

Of course, turbulence is not only important for commercial aviation, it also makes a fundamental contribution to the mixing of momentum and constituent species. The processes described here and the model simulations highlight the detailed spatial and temporal variability of this turbulent mixing. Despite the uncertainties in the representation of small-scale processes in numerical models, this study illustrates the potential value of mesoscale models in representing this turbulence for both fundamental and aviation applications. Moreover, although the small-scale and transient nature of turbulence implies that it has inherently low predictability, the results presented herein illustrate that turbulence is intimately tied to larger-scale resolved processes and characteristics of the basic unperturbed background flow that are more predictable.

*Acknowledgments.* We thank three anonymous reviewers for their constructive comments that helped improve the manuscript. The first author (TPL) was supported by a University of Melbourne Early Career Research grant. The second author (JDD) acknowledges support through the Office of Naval Research's Program Element 0601153N. Computational resources were supported in part by a grant of HPC time from the Department of Defense Major Shared Resource Center at Wright Patterson Air Force Base, OH. COAMPS is a registered trademark of the Naval Research Laboratory. Cyclone statistics were created using http://www.earthsci.unimelb.edu.au/tracks/cychome.htm; we thank Kevin Keay for his assistance. Figures 5c, 9c, and 14c were obtained from the NERC Satellite Receiving Station, Dundee University, Scotland (available online at http://www.sat.dundee.ac.uk/).

## REFERENCES

Bacmeister, J. T., and M. R. Schoeberl, 1989: Breakdown of vertically propagating two-dimensional gravity waves forced by orography. *J. Atmos. Sci.,* **46,** 2109–2134.

——, P. A. Newman, B. L. Gary, and K. R. Chan, 1994: An algorithm for forecasting mountain wave–related turbulence in the stratosphere. *Wea. Forecasting,* **9,** 241–253.

Booker, J. R., and F. P. Bretherton, 1967: The critical layer for internal gravity waves in shear flow. *J. Fluid Mech.,* **27,** 513–539.

Clark, T. L., and W. R. Peltier, 1984: Critical level reflection and resonant growth of nonlinear mountain waves. *J. Atmos. Sci.,* **41,** 3122–3134.

——, T. Keller, J. Coen, P. Neilley, H.-M. Hsu, and W. D. Hall, 1997: Terrain-induced turbulence over Lantau Island: 7 June 1994 Tropical Storm Russ case study. *J. Atmos. Sci.,* **54,** 1795–1814.

——, and Coauthors, 2000: Origins of aircraft-damaging clear air turbulence during the 9 December 1992 Colorado downslope windstorm: Numerical simulations and comparison to observations. *J. Atmos. Sci.,* **57,** 1105–1131.

Dörnbrack, A., 1998: Turbulent mixing by breaking gravity waves. *J. Fluid Mech.,* **375,** 113–141.

Doyle, J. D., and D. R. Durran, 2002: The dynamics of mountain-wave-induced rotors. *J. Atmos. Sci.,* **59,** 186–201.

——, and Q. Jiang, 2006: Observations and numerical simulations of mountain waves in the presence of directional wind shear. *Quart. J. Roy. Meteor. Soc.,* **132,** 1877–1905.

——, and Coauthors, 2000: An intercomparison of model-predicted wave breaking for the 11 January 1972 Boulder windstorm. *Mon. Wea. Rev.,* **128,** 901–914.

——, M. A. Shapiro, Q. Jiang, and D. L. Bartels, 2005: Large-amplitude mountain wave breaking over Greenland. *J. Atmos. Sci.,* **62,** 3106–3126.

Franke, P. M., and W. A. Robinson, 1999: Nonlinear behavior in the propagation of atmospheric gravity waves. *J. Atmos. Sci.,* **56,** 3010–3027.

Frehlich, R., and R. Sharman, 2004: Estimates of turbulence from numerical weather prediction model output with applications to turbulence diagnosis and data assimilation. *Mon. Wea. Rev.,* **132,** 2308–2324.

Fritts, D. C., and M. J. Alexander, 2003: Gravity wave dynamics and effects in the middle atmosphere. *Rev. Geophys.,* **41,** 1003, doi:10.1029/2001RG000106.

Grubišić, V., and P. K. Smolarkiewicz, 1997: The effect of critical levels on 3D orographic flows: Linear regime. *J. Atmos. Sci.,* **54,** 1943–1960.

Hodur, R. M., 1997: The Naval Research Laboratory's Coupled Ocean/Atmosphere Mesoscale Prediction System (COAMPS). *Mon. Wea. Rev.,* **125,** 1414–1430.

Jiang, Q., and J. D. Doyle, 2004: Gravity wave breaking over the central Alps: Role of complex terrain. *J. Atmos. Sci.,* **61,** 2249–2266.

Kalnay, E., and Coauthors, 1996: The NCEP/NCAR 40-Year Reanalysis Project. *Bull. Amer. Meteor. Soc.,* **77,** 437–471.

Kim, Y.-J., S. D. Eckermann, and H.-Y. Chun, 2003: An overview of past, present and future of gravity-wave drag parametrization for numerical climate and weather prediction models. *Atmos.–Ocean,* **41,** 65–98.

Lane, T. P., R. D. Sharman, R. G. Frehlich, and J. M. Brown, 2006: Numerical simulations of the wake of Kauai. *J. Appl. Meteor. Climatol.,* **45,** 1313–1331.

Lilly, D. K., 1978: A severe downslope windstorm and aircraft turbulence event induced by a mountain wave. *J. Atmos. Sci.,* **35,** 59–77.

——, and P. J. Kennedy, 1973: Observations of stationary mountain wave and its associated momentum flux and energy dissipation. *J. Atmos. Sci.,* **30,** 1135–1152.

Miles, J. W., and H. E. Huppert, 1968: Lee waves in a stratified flow. Part 2. Semi-circular obstacle. *J. Fluid Mech.,* **33,** 803–814.

Murray, R. J., and I. Simmonds, 1991: A numerical scheme for tracking cyclone centres from digital data. Part I: Development and operation of the scheme. *Aust. Meteor. Mag.,* **39,** 155–166.

Ólafsson, H., and H. Ágústsson, 2009: Gravity wave breaking in easterly flow over Greenland and associated low level barrier- and reverse tip-jets. *Meteor. Atmos. Phys.,* **104,** 191–197.

Peltier, W. R., and T. L. Clark, 1983: Nonlinear mountain waves in two and three spatial dimensions. *Quart. J. Roy. Meteor. Soc.,* **109,** 527–548.

Ralph, F. M., M. Crochet, and S. V. Venkateswaran, 1992: A study of mountain lee waves using clear-air radar. *Quart. J. Roy. Meteor. Soc.,* **118,** 597–627.

——, P. J. Neiman, T. L. Keller, D. Levinson, and L. Fedor, 1997: Observations, simulations, and analysis of nonstationary trapped lee waves. *J. Atmos. Sci.,* **54,** 1308–1333.

Roe, G. H., 2005: Orographic precipitation. *Annu. Rev. Earth Planet. Sci.,* **33,** 645–671.

Schwartz, B., 1996: The quantitative use of PIREPs in developing aviation weather guidance products. *Wea. Forecasting,* **11,** 372–384.

Sharman, R. D., and M. G. Wurtele, 2004: Three-dimensional structure of forced gravity waves and lee waves. *J. Atmos. Sci.,* **61,** 664–680.

——, C. Tebaldi, G. Wiener, and J. Wolff, 2006: An integrated approach to mid- and upper-level turbulence forecasting. *Wea. Forecasting,* **21,** 268–287.

Shutts, G., 1995: Gravity-wave drag parametrization over complex terrain: The effect of critical-level absorption in directional wind-shear. *Quart. J. Roy. Meteor. Soc.,* **121,** 1005–1021.

Smith, R. B., and V. Grubišić, 1993: Aerial observations of Hawaii's wake. *J. Atmos. Sci.,* **50,** 3728–3750.

Smolarkiewicz, P. K., and R. Rotunno, 1989: Low Froude number flow past three-dimensional obstacles. Part I: Baroclinically generated lee vortices. *J. Atmos. Sci.,* **46,** 1154–1164.

Thorpe, S. A., 1975: The excitation, dissipation, and interaction of internal waves in the deep ocean. *J. Geophys. Res.,* **80,** 328–338.

——, 1987: Transitional phenomena and the development of turbulence in stratified fluids: A review. *J. Geophys. Res.,* **92** (C5), 5231–5248.

Uhlenbrock, N. L., K. M. Bedka, W. F. Feltz, and S. A. Ackerman, 2007: Mountain wave signatures in MODIS 6.7-$\mu$m imagery and their relation to pilot reports of turbulence. *Wea. Forecasting,* **22,** 662–670.

Wolff, J. K., and R. D. Sharman, 2008: Climatology of upper-level turbulence over the contiguous United States. *J. Appl. Meteor. Climatol.,* **47,** 2198–2214.

Wurtele, M. G., R. D. Sharman, and A. Datta, 1996: Atmospheric lee waves. *Annu. Rev. Fluid Mech.,* **28,** 429–476.